



Electrochemical detection combined with artificial neural networks for the simultaneous intelligent sensing of caffeine and chlorogenic acid

Bing-Chen Gu^a, Kuan-Jung Chung^b, Bo-Wei Chen^c, Yu-Han Dai^d, Chia-Che Wu^{c,*}

^a Doctoral Program in Semiconductor and Green Technology, Academy of Circular Economy, National Chung Hsing University, 250, Taichung, 402, Taiwan

^b Department of Mechatronics Engineering, National Changhua University of Education, 250, Taichung, 402, Taiwan

^c Department of Mechanical Engineering, National Chung Hsing University, 250, Taichung, 402, Taiwan

^d Vida BioTechnology Co., Ltd. Taiwan, 145 Xingda Rd., South Dist., Taichung, 402, Taiwan

ARTICLE INFO

Keywords:

Electrochemistry
Machine learning
Caffeine
Chlorogenic acid

ABSTRACT

Caffeine (CAF) is a common central nervous system stimulant. However, the excessive intake of CAF can cause physical discomfort to consumers and affect the health of drinkers. Chlorogenic acid (CGA) is a powerful antioxidant with antiinflammatory and antiobesity properties. Here, we used an artificial neural network (ANN) for the intelligent sensing and electrochemical measurements of CAF and CGA by differential pulse voltammetry and linear sweep voltammetry. The measurement error of the electrochemical method for detecting CAF concentrations could be eliminated using a large amount of electrochemical measurement data for ANN training. The CAF and CGA concentrations were sensed with an accuracy of nearly 90%. A sample of real coffee was also sensed with an accuracy rate of over 90%. The results showed that this method can effectively eliminate the errors of electrochemical measurement methods and instruments, and the accuracy rate of calibration line measurements exceeded that of the traditional electrochemical method.

1. Introduction

Tea and coffee liquids contain caffeine (CAF), which has a refreshing effect. CAF is a central nervous system stimulant of the class of methylxanthines, and its molecular shape is similar to that of adenosine [1]. Adenosine is a purine nucleoside comprising adenine molecules linked to a ribofuranose moiety by a β -N9-glycosidic bond. Adenosine is a neuromodulator that has an inhibitory effect on the central nervous system. When adenosine binds to its receptors, it can inhibit the release of certain neurotransmitters, which can produce an anticonvulsant with a sedative effect. Considering that the molecular shape of CAF is similar to that of adenosine, the receptors of adenosine will, in turn, bind to CAF molecules, reducing and blocking the effect of adenosine on its receptors, thereby preventing adenosine-induced somnolence [2]. The European Committee of Experts on Food Science has recommended a daily CAF intake of less than 400 mg for adults [3]. For healthy adults, the U.S. Food and Drug Administration has also cited 400 mg a day as an amount that is not generally associated with dangerous and negative effects. Another chemical called chlorogenic acid (CGA) is found in high concentrations in coffee, around 70–350 mg per cup of coffee. CGA has good functions that can help people to prevent cardiac disease. CGA is

also a good antioxidant that can decrease inflammation in cells and improve the efficiency of cells to metabolize carbohydrates, to stabilize glucose levels in human bodies [4]. An understanding of the amount of CAF and CGA can help consumers to choose the coffee.

The commonly used CAF test in beverages is high-performance liquid chromatography (HPLC) [5,6], which requires the use of HPLC detectors and chromatography columns. HPLC, a gold standard in detecting CAF and CGA, has the advantages of high sensitivity and accuracy. However, the sample preparation procedure, which requires a well-trained technician, is typically time-consuming and rate-limiting. Moreover, the cost of test equipment and reagents is relatively expensive. The availability of HPLC in a coffee store or at home is very improbable. Measuring CAF or CGA levels at home or in a coffee shop can be crucial for quality control, health considerations, and labeling requirements. The quantity of CAF and CGA extracted from coffee beans is influenced by various factors, including the brewing method, temperature, and time, even while using the same beans. Recently, the development of portable caffeine detection tools has received significant attention. Ramos et al. [7] showed that caffeine could be selectively determined in complex samples using a portable flow system with amperometric detection. Xu et al. [8] fabricated an aqueous caffeine fluorescent sensor, which can

* Corresponding author at: Department of Mechanical Engineering, National Chung Hsing University, Taichung, 40227, Taiwan.

E-mail address: josephwu@dragon.nchu.edu.tw (C.-C. Wu).

excite caffeine with a high selectivity of 250-fold fluorescence enhancement via nuclear magnetic resonance and Fourier transform infrared spectroscopies. This method has high sensitivity and selectivity but still requires large-scale equipment.

Voltammetry using disposable electrodes has the advantages of speed, cost-effectiveness, high sensitivity, miniaturization, and portable detection and can be used to detect microsubstances in solution. Benalte et al. [9] used screen-printed gold electrodes to detect mercury content in water, and the sensitivity reached 1.1 ng/mL. Renedo et al. [10] used a carbon electrode modified with gold particles to detect the concentration of oxalate (SbIII) in water, and the detection limit reached 9.33×10^{-10} M Tadesse et al. [11] fabricated an anthraquinone-modified carbon paste electrode (AQM-CPE) and studied its effect on CAF oxidation by cyclic voltammetry (CV). Square wave voltammetry was employed to plot a calibration curve, and the anodic peak current had a good linear relationship with the CAF concentration in the range of 2×10^{-6} to 4×10^{-8} M with a correlation coefficient of 0.998 and a detection limit of 1.43×10^{-7} M Sun et al. [12] used a Nafion-modified glassy carbon electrode (Nafion-Gr/GCE) to analyze coffee using electrochemical methods, such as CV and differential pulse voltammetry (DPV). During the CV experiment, 0.01 M electrolyte sulfuric acid (H_2SO_4), nitric acid (HNO_3), acetic acid (CH_3COOH), and hydrochloric acid (HCl) were used as supporting electrolytes. The highest electrochemical response was realized with a supporting electrolyte of 0.01-M H_2SO_4 . H_2SO_4 reagents with pH levels in a range of 0.5–2.0 were tested, and the peak potential decreased with an increase in pH. In our previous study [13], we described the development of an electrochemical sensor for *Escherichia coli* detection. The sensor used disposable biochips with a gold working electrode, a carbon counter electrode, and an Ag/AgCl reference electrode. Besides, another study [14] introduced a biosensor for A β (1–42) conformation detection, employing disposable chips with gold nanoparticles deposited on a nanostructured gold electrode.

Although these electrochemical sensors can be used to detect CAF and CGA, the cyclic voltammograms of different batches of disposable electrodes and different waiting times might vary. The electrode sizes at different locations for different manufacturing batches might vary. Harris [15] fabricated a carbon ink electrode and observed its poor reproducibility. The surface of the electrode was rough and highly heterogeneous with random arrays of carbon particles of different sizes, causing variable resistance, capacitance, or electroactive area. Additionally, the different waiting times might have resulted in different electrochemical signals. Chen et al. [16] developed a method for the electrochemical detection of vanillin and discovered that the oxidation peak of vanillin increased from 0 to 8 min of waiting time. Han et al. [17] experimentally observed a time-dependent electrical double layer in an electrolyte. They observed that to develop a fully electrical double layer with a large potential, they should wait for more than 0.05 s for their experimental setup. The voltammograms were dependent on the distribution of the electrical double layer relative to the sizes of the electrodes and waiting time. The commercialization of electrochemical sensors with screen-printed electrodes with such challenges will lead to poor repeatability and durability.

Machine learning has received considerable attention in the last two decades in dealing with mass data analysis. Through mass data learning, a computer can build an algorithm to reduce measurement deviation [18–20]. Zhao et al. [21] reported an artificial intelligence (AI) system for improving the electrochemical multicomponent detection of insulin and glucose. A database containing inputs and outputs was used to build a regression model to resolve the overlapping peak problem. Blanco et al. [22] combined organic electrosynthesis with ANNs to improve electrosynthesis conditions to 30% and 325% in the electrosynthesis of adiponitrile production rates and selectivity, respectively. Alharbi et al. [23] reported surface-enhanced Raman scattering combined with an ANN to detect caffeine and its two major metabolites, theobromine and paraxanthine. A bootstrapping random resampling procedure was employed to reduce the deviation of Raman spectroscopy. Chen et al.

[24] used a multiheaded dense neural network to quantitatively analyze the reduction of acetic acid in an aqueous solution, generating thermodynamic and kinetic data. They suggested that the AI approach allowed the extraction of parameters independent of the experimenter, thereby facilitating interlaboratory comparisons.

Here, an electrochemical sensor combined with an ANN was developed for the intelligent sensing of CAF and CGA. The experimental procedure is shown in Fig. 1(a). First, a drop of coffee was extracted and mixed with an electrolyte. Second, disposable electrodes with a portable electrochemical analyzer were used to perform linear sweep voltammetry (LSV) and DPV. The features were extracted from the DPV and LSV results and used to train an ANN. An ANN model was built with appropriate activation and loss functions for data training. The CAF and CGA concentrations were modeled and accurately calibrated by machine learning. Finally, the CAF and CGA results were shown in the app on electronic devices, such as a cellular phone or PAD via Bluetooth. AI was used to model the multiple features in the voltammogram and analyze the relationships between these features. Furthermore, the variations in the electrochemical results for different manufacturing batches and waiting times were calibrated by the developed ANN model, which will speed up the commercialization of the CAF and CGA analyzer.

2. Materials and methods

2.1. Chemicals

All the chemicals used were of analytical grade and used without further purification. The CAF and CGA were obtained from Sigma-Aldrich (USA). Phosphate-buffered solution and sulfuric acid were purchased from Echo Chemical (Taiwan). Coffee beans were purchased from Blossom Valley International (Taiwan). A real coffee sample was prepared from the coffee beans, which were first ground to powder, and 40 g of the powder was soaked in water at 90 °C for 5 min. All the chemical solutions were prepared with double-deionized water (DDW) were performed at 25 °C (± 2 °C).

The disposable electrochemical chips were fabricated on the printed circuit boards (PCB). The graphite electrode as the working electrode, graphite electrode as the counter electrode and Ag/AgCl electrode as the reference electrode were then screen printed on the PCB. The biocompatible glue which was purchased from PERMA Enterprise (Taiwan) was then dispensed on the electrochemical chips to form a wall to enclose working, counter and reference electrodes. The wall can be used to avoid sample spillage and to reduce the error. The electrochemical chips were used for testing only once without any surface modification. We added 0.1 ml of the standard or real sample to 0.9 mL of DDW and mixed them by vortex for 10 s. Subsequently, 0.1 mL of the diluted solution was mixed with 0.9 mL of a sulfuric solution with a concentration of 0.05 M by vortex for 10 s. Finally, 0.2 mL of the mixed solution was dropped on the disposable electrochemical chips for the following electrochemical tests.

2.2. Instruments

All the electrochemical experiments were performed with a VBS-100 portable electrochemical workstation purchased from VidaBio Technology (Taiwan). LSV and DPV were implemented. For LSV, the sweep voltage range, sweep rate, and initial voltage were 0–800 mV, 50 mV/s, and 50 mV, respectively. For DPV, the sweep voltage range and initial voltage were 0–1600 mV and 0 V, respectively. The pulse height, pulse width, step height, and step time are 5 mV, 5 ms, 5 mV, and 300 ms, respectively. The scan factors of LSV and DPV were already optimized. An electronic balance was purchased from Sartorius (Germany). The CAF standard test was performed by HPLC (JTTEC Service Corporation, Taiwan), and the CGA standard test was performed by HPLC at Chia Nan University of Pharmacy and Science (Taiwan) for comparison.

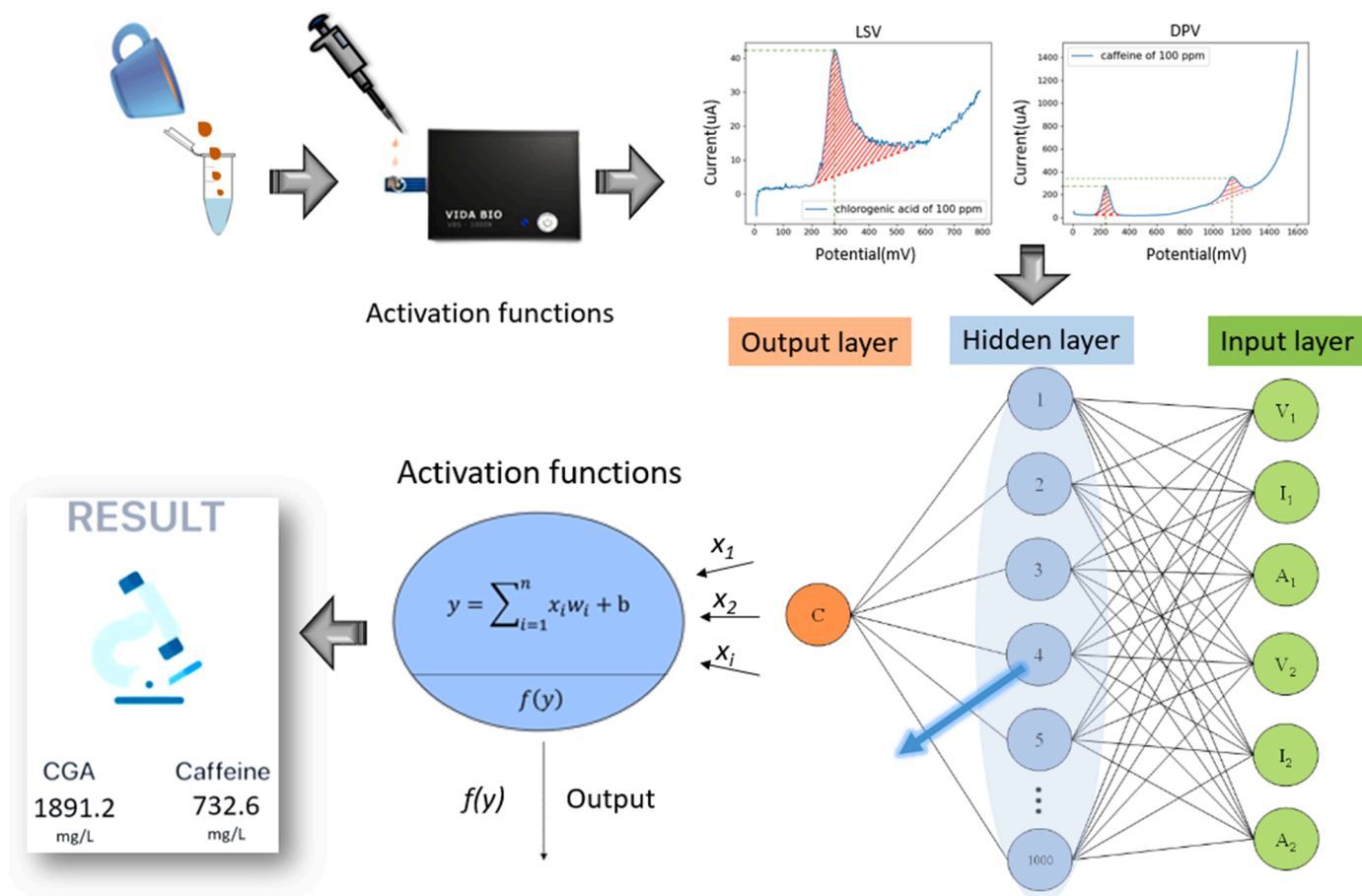


Fig. 1. (a) Experimental procedure.

2.3. Feasibility study

To simultaneously detect CAF and CGA in a single disposable electrochemical chip, LSV and DPV were employed. For CAF sensing, Tajew et al. [25] used a GCE modified with an attapulgite/Nafion film by CV and DPV. They observed that caffeine exhibited an irreversible oxidation peak around +1.41 V (vs. Ag/AgCl reference electrode) in 0.1-M H₂SO₄ at a pH of 1.5 because of the strong antioxidant properties of CAF. The reaction equation for CAF involves the transfer of 4 protons and 4 electrons as depicted in Fig. 2a. The initial step of this pathway, where caffeine (CAF) is converted to either trimethyl uric acid (TMU (I) or TMU (II)), may be mediated by caffeine oxidases that are currently not well characterized. The disposable electrochemical chip with graphite working and counter electrodes and an Ag/AgCl reference electrode was

used to reduce the complexity of the fabrication process without further modification. Here, 0.01-M H₂SO₄ was used for safety and the waste recycling of consumer products. Namazian et al. [26] employed CV, chronoamperometry, and rotating disk electrode voltammetry to quantify CGA using a glassy carbon disk as a working electrode, a graphite bar as a counter electrode, and a saturated calomel electrode (SCE) as a reference electrode. They observed that CGA exhibited an irreversible oxidation peak around 0.617 V (vs. SCE). The electrochemical behavior of CGA was strongly dependent on the solution pH. Fig. 2b illustrates the oxidation process of CGA. CGA can undergo oxidation, resulting in the formation of CGA-ox and various oxidized products that possess unique chemical properties. CGA had a relatively lower oxidation potential than CAF. Here, a single sweep of LSV, followed by a single sweep of DPV, was performed on the disposable

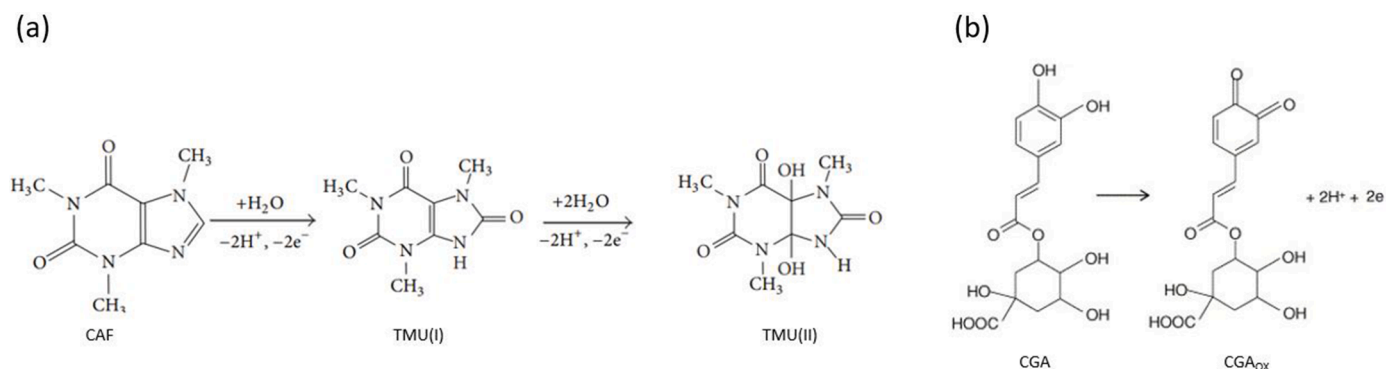


Fig. 2. Oxidation mechanisms of (a) caffeine and (b) chlorogenic acid.

electrochemical chip to simultaneously quantify CAF and CGA.

The oxidation potential of CGA around 0.25 V (vs. Ag/AgCl reference electrode) was considerably smaller than that of CAF around 1.05 V. The characteristic oxidation peaks of CGA were measured by LSV within a sweep voltage range of 0–800 mV. However, when the voltage exceeded 800 mV, the nonFaraday (capacitive) current significantly affected the CAF measurements during the experiment. DPV was employed to reduce the nonFaraday current and quantify CAF by measuring the current immediately before the increasing base potential between pulses with equal increments. After LSV measurements, DPV was employed to sweep from 0 to 1600 mV. The features of LSV and DPV were used to quantify CGA and CAF.

2.4. Machine learning model

Machine learning is aimed at finding out rules from a large amount of data. Machine learning was employed to reduce variations when different electrochemical modes were continually applied on the same working electrode. Using a suitable algorithm, a set of machine learning models were established to discover or predict trends. The most widely used machine learning method is supervised learning, which is a technology that allows machines to use the experience under supervision. The construction of the supervised machine learning model originates from the establishment of a dataset for input and predictive (actual) values. The input and predictive values can be as simple as numbers, matrices, vectors, or more complex pieces of text, pictures, or even DNA sequences. Thereafter, a suitable algorithm is used to analyze the existing data to establish a model that can judge or predict new data. For supervised learning, ANN is one of the most powerful tools for classification, recognition, and prediction. ANN is a model similar to the human nervous system, which simulates the transmission and calculation of neurons. ANN is considerably more powerful and useful compared with traditional regression and statistical models.

Here, an ANN was developed using an open-source machine learning library in Tensorflow. The ANN was mainly divided into three parts, which are the input, hidden, and output layers. The input layer represents the input value mentioned in the preceding paragraph, which is the basis for the model to judge, whereas the hidden layer is mainly used by the ANN. The calculation part is the key to connecting the input and output layers. The output layer is the prediction of the actual value by the model, representing the result of the model prediction. Each neuron is only connected to the upper and lower layers, independent of other neurons in the same layer. It is similar to the human nervous system. The brain calculates data and foresees the target by signal transmission between nerves. The input layer represents the collection of input values, and the hidden layer is responsible for calculating the input values.

It is also like the critical joint, which links the input and output layers. The output layer shows the target values by prediction. Each neuron only connects the former layer and the next layer, and every neuron is independent in the same layer. A neuron stands for the input factor weight and activation function shown in Fig. 1(b). The equation of activation function is shown below.

$$y = \sum_{i=1}^n x_i w_i + b \quad (1)$$

y , x_i , w_i , and b are the output value, input value, weighting coefficient, and model bias, respectively.

The output of y was calculated by activation functions before transmitting to the next ANN layer. Eq. (1) shows a linear equation. The nonlinear equation was produced by activation function processing to deal with nonlinear data. A single neuron can already predict target values by input values. The network of multiple neurons is built to solve linear or nonlinear equations to increase the accuracy of prediction with a complicated database [27]. The activation functions can help the ANN model to solve linear and nonlinear equations between each neuron. The

rectified linear unit is applied to the activation function to solve the relationship between the concentration and characteristic signal. It maps the resulting values between 0 and 1 or -1 and 1 etc. Here, an output value was obtained by neuron calculation. This value could be very different from the real value, which we exempted. The difference between output and real values is called the loss function. The loss function is inputted into the optimizer to generate a new loss function, and the new loss function is inputted to the neurons to change the weighting coefficients to reduce the loss function in the next input value, which is inputted to the ANN model. The goal of the ANN is to produce the minimum loss function. The loss function obtained by Huber [28] was used in the present study. The Huber loss function can improve the robustness of the squared loss function. The squared loss function is too sensitive for outliers. The Huber loss function can combine the mean squared error and absolute value functions. By operating the ANN model, the optimizer changed the weighting coefficients through repeated training. The optimizer developed by Nadam. [29,30] was utilized. When the loss function approached convergence, the ANN model stopped training. The reliability could be obtained by comparing the training and testing sets. The quality of the ANN model was generally determined using the mean absolute error (MAE) and root-mean-square error (RMSE). The electrochemical plot comprised large data points. Here, the data of the feature peak was discovered and defined before data was inputted into the training set. A difference of less than 10% between the predicted and true values was regarded as a correct prediction. The definition of accuracy in this study was how much percentage of data was in this range.

2.5. Database collection

Here, 14 different concentrations of CAF and CGA each were prepared. The same concentrations of CAF and CGA were prepared in sample test tubes as standard solutions. They were 100, 500, 1000, 1500, 2000, 2500, 3000, 4000 and 5,000 mg/L. The commercial coffee samples were tested via HPLC in a chemical lab. The HPLC results served as a reference for commercial coffee. These samples were tested using electrochemical methods at the same time.

All the electrochemical experiments were conducted with sensors and the VBS-100 portable electrochemical workstation. Electrochemical plots were imported from the VBS-100 graphing software. The CGA oxidation peak was observed near 300 mV, and the CAF oxidation peak was observed near 1200 mV in the DPV plot. We developed an algorithm to find the maximum from 100 to 300 mV and integrated the curve area between 100 and 300 mV. We denoted the maximum peak potential of CGA by CAF-V₁, the maximum peak current of CGA by CAF-I₁, and the integrated area of CGA by CAF-A₁ in the DPV plot. The CAF oxidation peak was observed near 1200 mV. We developed an algorithm to find the maximum from 1000 to 1300 mV and integrated the curve area between 1000 and 1300 mV. We denoted the maximum peak potential of CAF by CAF-V₂, the maximum peak current of CAF by CAF-I₂, and the integrated area of CAF by CAF-A₂ in the DPV plot. The future peak of CGA in the DPV plot inputted into the ANN model could help to increase prediction accuracy. The CGA oxidation peak was observed near 300 mV in the LSV plot. We developed an algorithm to find the maximum from 200 to 550 mV and integrated the curve area between 200 and 550 mV. We denoted the maximum peak potential of CGA by CGA-V₁, the maximum peak current of CGA by CGA-I₁, and the integrated area of CGA by CGA-A₁ in the LSV plot. The CGA oxidation peak was also observed near 300 mV in the DPV plot. We developed an algorithm to find the maximum from 100 to 300 mV and integrated the curve area between 100 and 300 mV. We denoted the maximum peak potential of CGA by CGA-V₂, the maximum peak current of CGA by CGA-I₂, and the integrated area of CGA by CGA-A₂.

After all the feature values were calculated, the values were normalized. The data was mapped from 0 to 1, as shown in Eq. (2).

$$x_{normalization} = (x - x_{min}) / (x_{max} - x_{min}) \quad (2)$$

Thereafter, the six feature values of CAF were assigned a dataset. The CAF training set of the standard solutions and real samples contained 701 cases, and the CAF test set of the standard solutions and real samples contained 175 cases shown in Table 1. The final concentrations were the values of the output layers. Here, 1000 neurons were between the input and output layers. The CAF ANN model was completed after 10,000 training times. The six feature values of CGA were assigned a dataset. The CGA training set of the standard solutions and real samples contained 428 cases, and the CGA test set of the standard solutions and real samples contained 107 cases shown in Table 1. The concentrations were the values of the output layers. Here, 1000 neurons were between the input and output layers. The CGA ANN model was also completed after 10,000 training times.

3. Results and discussion

3.1. ANN model prediction

Figure 3a shows the LSV plot of different CGA concentrations. When CGA increased, a large oxidation peak was observed near 300 mV. The observed peak values were 8.1, 22.0, 39.7, 56.9, 75.2, 92.1, 109.2, 144.8, and 181.3 μA for CGA concentrations of 100, 500, 1000, 1500, 2000, 2500, 3000, 4000 and 5,000 mg/L, respectively. The blank solution without CGA did not exhibit any peaks.

Figure 3b shows the DPV plot of different concentrations of CGA and CAF. The peak values of CGA were observed at approximately 68.2, 188.1, 279.5, 368.3, 467.1, 501.8, 529.9, 555.6, and 623.2 μA , for CGA concentrations of 100, 500, 1000, 1500, 2000, 2500, 3000, 4000 and 5,000 mg/L, respectively, near 300 mV. Additionally, a significant oxidation peak was observed at around 1100 mV only when the concentration of CAF increased. The peak values for CAF were measured at 189.2, 254.8, 339.1, 422.3, 505.9, 588.7, 673.2, 840.1 and 1005.8 μA for concentrations of 100, 500, 1000, 1500, 2000, 2500, 3000, 4000 and 5,000 mg/L, respectively. Importantly, no peaks were observed in the blank solution where neither CAF nor CGA was present. Fig. 3 provides a visual representation of the distinct electrochemical signals of caffeine and chlorogenic acid at different concentrations. Changes in concentration can influence the oxidation current, allowing for the differentiation and definition of the characteristic signals of caffeine and chlorogenic acid.

For the CAF training set, there are a total of 701 data points, with 526 points corresponding to standard caffeine solution concentrations and 175 points representing real coffee samples. The concentrations of the real coffee samples in the training set were determined using HPLC. A linear regression equation was derived from the values of CAF-I₂ with the CAF concentrations from 100 to 5,000 mg/L. The equation for the linear regression line is $y = 1.670x + 171.8$, with an coefficient of determination R² value of 0.94. The test set comprises 175 data points, with 116 points representing standard caffeine solution concentrations and 59 points representing real coffee samples. Similar to the training set, the concentrations of the real coffee samples in the test set were determined using HPLC. The concentrations of the test samples were

Table 1
CAF and CGA model cases.

CAF	
Set	Case
Training set	701 (contains 285 real samples)
Test set	175 (contains 59 real samples)
CGA	
Set	Case
Training set	428 (contains 24 real samples)
Test set	107 (contains 6 real samples)

calculated using the linear regression equation derived from Fig 4(a). Fig. 4(b) displays the plotted values of calculated and real concentrations of CAF for the training set. The RMSE for the prediction is 59.39, and the MAE is 47.809. Notably, poor predictions were observed for samples with concentrations exceeding 230 mg/L.

Simultaneously, the measurement results from the training set were utilized in the ANN model. After 10,000 training iterations and a training time of 140 min, a caffeine-specific ANN model was developed. The predicted concentrations were compared to the real concentrations for the samples from the training set, as illustrated in Fig. 4(c). The RMSE was calculated to be 2.77, and the MAE was 2.05. Subsequently, the concentrations of the samples from the test set were calculated using the ANN model depicted in Fig 4(c). The predicted concentrations were then compared to the real concentrations for the test set samples, as displayed in Fig. 4(d). The RMSE for this comparison was found to be 10.20, with a corresponding MAE of 7.01. The results demonstrate that the ANN models exhibit high potential in accurately predicting CAF concentrations.

The CGA training set comprises a total of 428 data points, with 404 points representing standard caffeine solution concentrations and 24 points representing real coffee samples. The concentrations of the real coffee samples in the training set were determined using HPLC. A linear regression equation was derived from the CGA training set, as shown in Fig. 5(a), to establish a relationship between the values of CGA-I₁ and the CGA concentrations. The equation for the linear regression line is $y = 0.350x + 4.954$, with an R² value of 0.97. The test set consists of 117 data points, with 111 points representing standard caffeine solution concentrations and 6 points representing real coffee samples. Similar to the training set, the concentrations of the real coffee samples in the test set were determined using HPLC. The concentrations of the test set samples were calculated using the linear regression equation derived from Fig 5(a). Fig. 5(b) depicts the comparison of calculated and real concentrations of CAF for the training set. The RMSE for the prediction is 36.74, and the MAE is 26.84. Notably, poor predictions were observed for samples with concentrations of 127 and 179 mg/L.

The measurement results from the training set were also utilized in the ANN model. Following 10,000 training iterations and a training time of 75 min, a caffeine-specific ANN model was developed. The predicted concentrations were compared to the real concentrations for the samples from the training set, as illustrated in Fig. 4(c). The RMSE was found to be 4.10, and the corresponding MAE was 2.87. Additionally, the concentrations of the samples from the test set were calculated using the ANN model shown in Fig 4(c). The predicted concentrations were then compared to the real concentrations for the test set samples, as displayed in Fig. 4(d). The RMSE for this comparison was found to be 6.31, with a corresponding MAE of 4.48. These results indicate the potential of the ANN models in accurately predicting CAF concentrations.

3.2. ANN model developed for different fabrication batches of sensors

Specific electrochemical signals were observed among four fabrication batches of sensors. Alterations in the fabrication process can introduce unknown factors that are challenging to control consistently over different batches. One such factor is fabrication tolerance, which can contribute to the size variations in the electrochemical electrodes, producing consequent variations in observed electrochemical signals. Figs. 6(a) displays plots obtained from four samples of different fabrication batches using the LSV technique, whereas Fig. 6(b) presents plots obtained using DPV. Notably, the electrochemical features observed in Figs. 6(a) and (b) differ from each other for different batch. The accuracy of CAF and CGA measurements for sensors from different fabrication batches is found to be poor when employing a linear regression equation. This indicates that the linear regression equation may not be effective in estimating the variations introduced by different fabrication batches.

We conducted experiments using six different concentrations of CAF

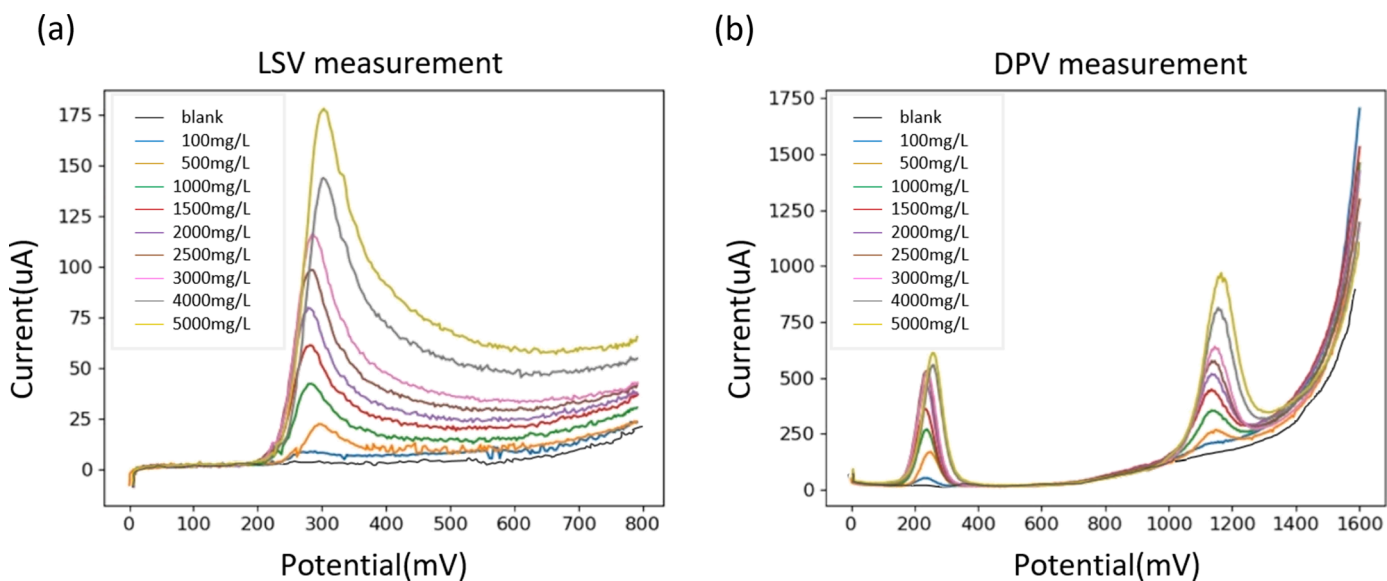


Fig. 3. (a) The plot of LSV measurement for different CGA concentrations (b) The plot represents the DPV measurements for different concentrations of CAF and CGA.

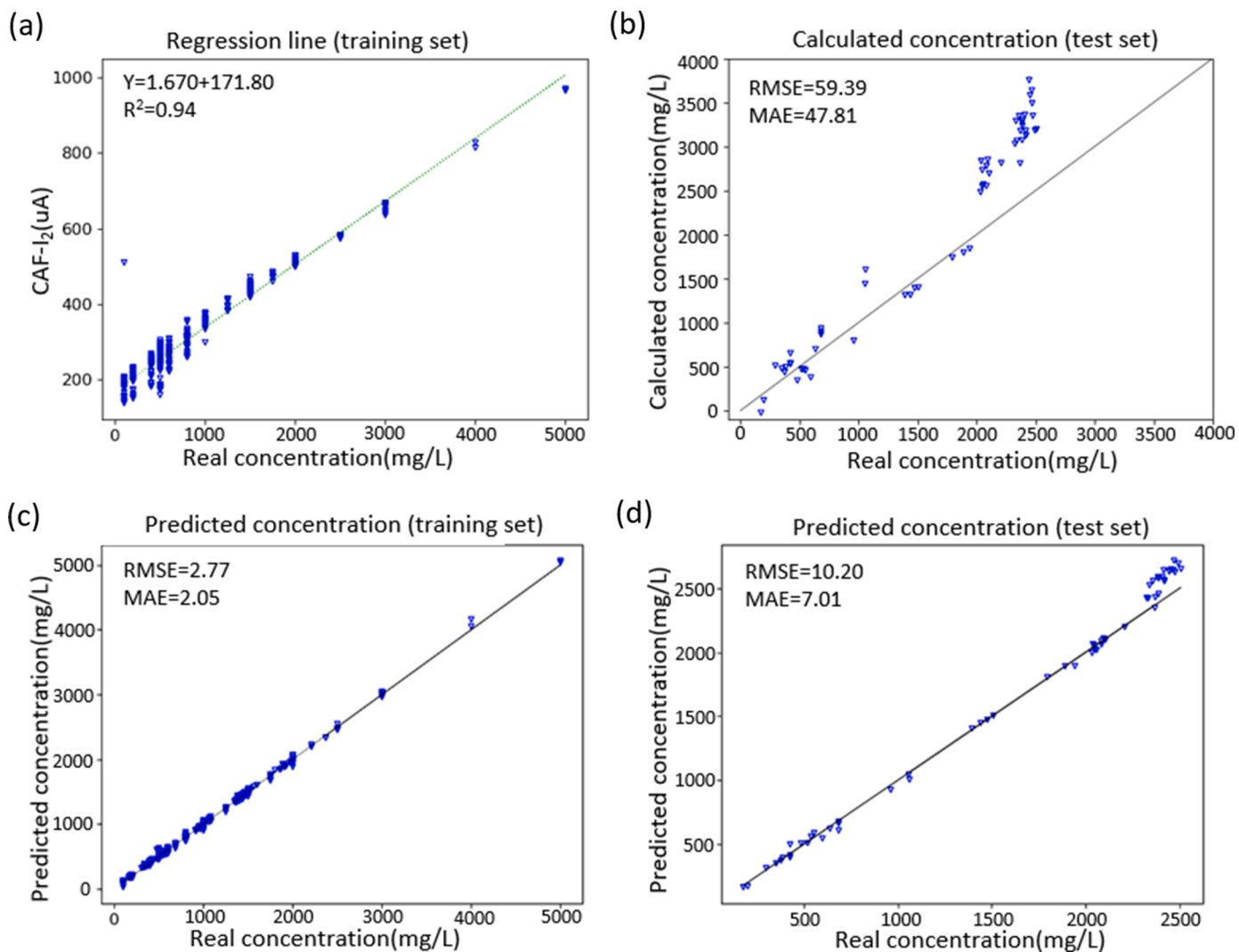


Fig. 4. (a) Linear regression line for CAF training set, (b) calculated results using linear regression equation for CAF test set, (c) predicted concentration using ANN model for CAF training set, and (d) predicted results using ANN model for CAF test set.

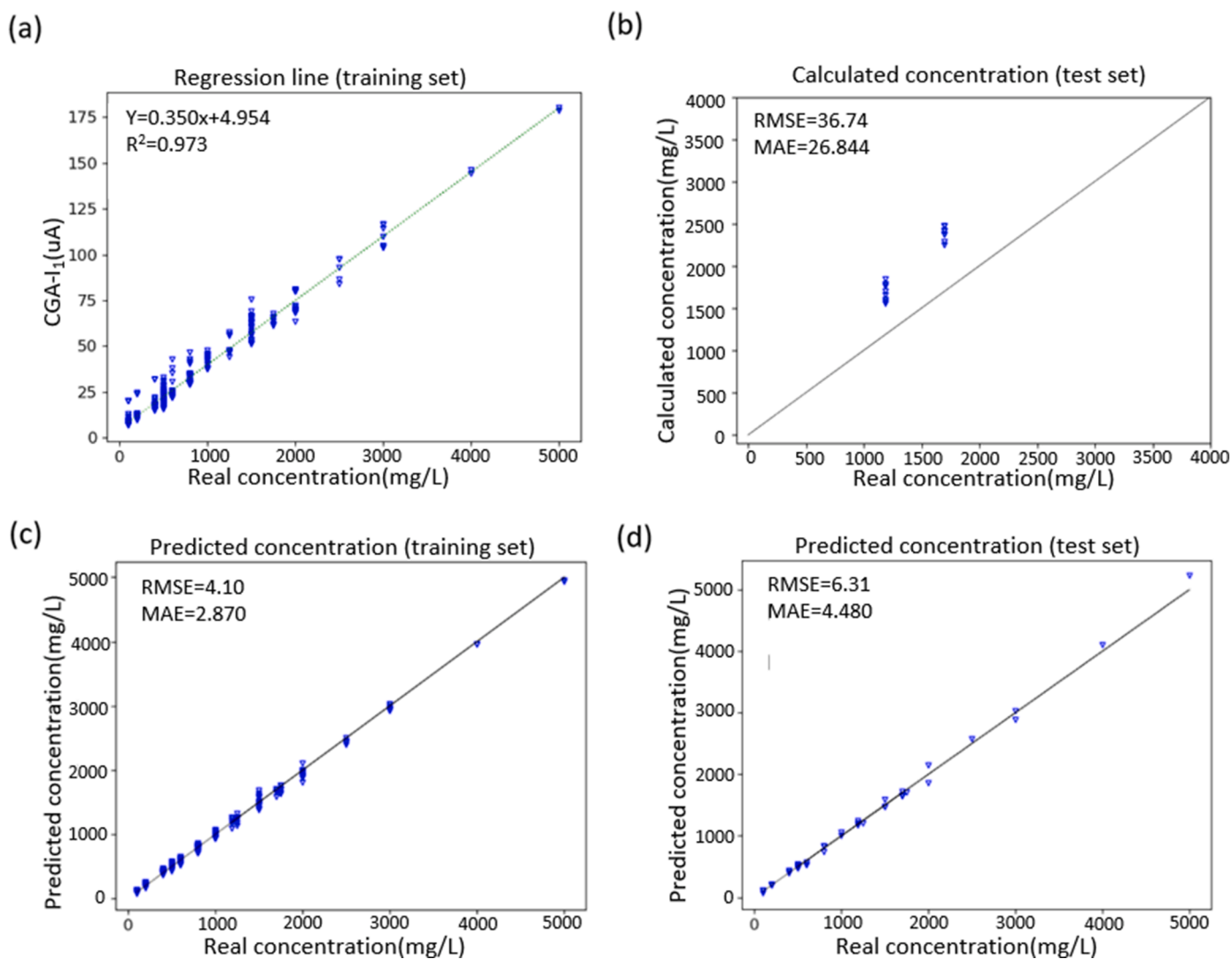


Fig. 5. (a) The linear regression line for the CGA training set, (b) calculated results using linear regression equation for the CGA test set, (c) predicted concentration using ANN model for the CGA training set, and (d) predicted results using ANN model for the CGA test set.

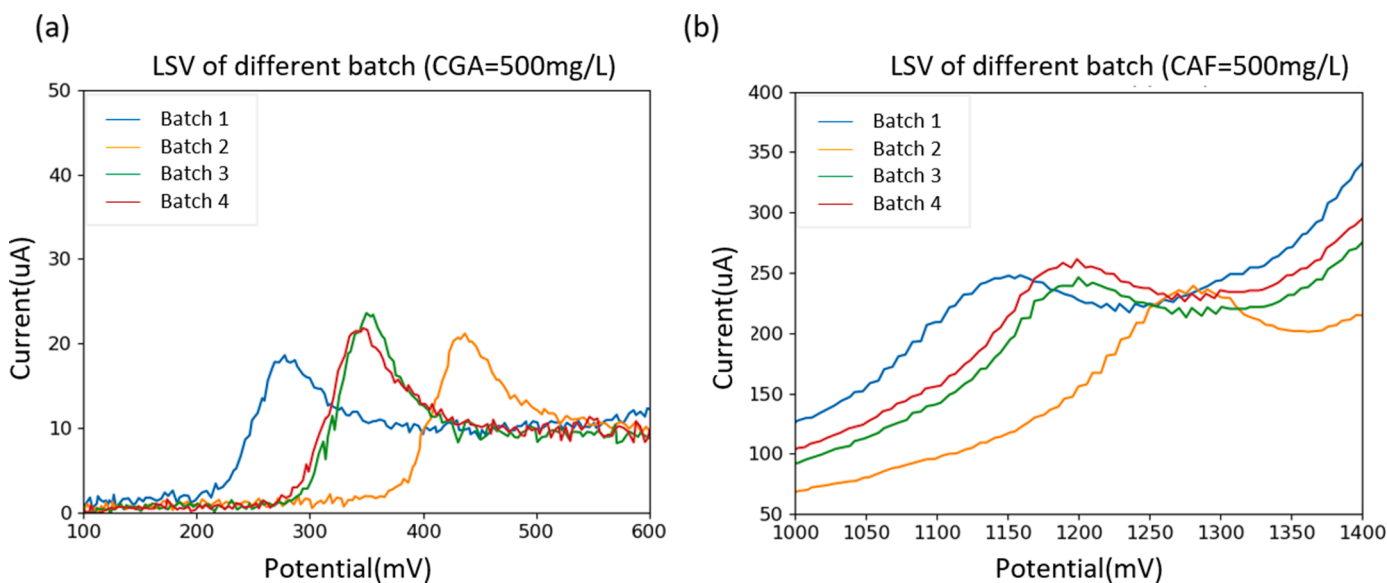


Fig. 6. (a) The plots of the LSV measurement for four samples from different fabrication batches. (b) The plot of the DPV measurement for four samples from different fabrication batch.

and CGA of four different fabrication batches of sensors. Each fabrication batch comprised 120 sensors. To analyze the data, we constructed four linear regression models using CAF and CGA sensors from each respective fabrication batch. Figs. 7(a) displays the results for the CAF measurement, showing the values of R^2 for each fabrication batch. The R^2 values for batches 1, 2, 3 and 4 were found to be 0.96, 0.97, 0.95 and 0.97, respectively. These R^2 values indicate the degree of correlation between the measured CAF concentrations and the predictions made by the linear regression lines for each fabrication batch. Each linear regression equation exhibits a reasonable coefficient of R^2 for individual fabrication batches. However, when combining all sensors from batches of 1, 2, 3 and 4, the overall R^2 decreases to 0.92, as depicted in Fig. 7(c). For the CGA measurement, Fig. 7(c) reveals the values of R^2 for each fabrication batch. Batch 1, 2, 3 and 4 exhibited R^2 values of 0.97, 0.71, 0.98 and 0.99, respectively. Except for batch 3, each linear regression equation describes favorable results in terms of the R^2 . However, when combining the results from all four fabrication batches to construct a single linear regression line, the R^2 decreases considerably to 0.69. This challenge was overcome by the ANN model. Figs. 7b and 7d show that four batches of data could be predicted using the ANN model. Table 2 show that the RMSE and MAE of CAF in the four batches of sensors were

Table 2

Comparison of calibration linear model and ANN model for four different fabrication batches.

	Calibration line model (CAF)	ANN model (CAF)	Calibration line model (CGA)	ANN model (CGA)
MAE	200.59	1.54	22.59	1.99
RMSE	201.49	2.14	27.01	2.85
Accuracy (%)	40.3	91.7	37.5	77.7

2.14 and 1.54, respectively. The RMSE and MAE of CGA in the four batches of sensors were 2.85 and 1.99, respectively. The CAF accuracy was improved from 40.3% to 91.7%, and the CGA accuracy was improved from 37.5% to 77.7%.

The mechanism of the electrochemical sensor is applying different potentials to the electrodes. Electrochemical reactions occur near the electrode surface. Here, the working electrode was printed using graphite. When different batches of sensors were produced, different electrochemical features were generated because it was difficult to control the conditions to be the same in different manufactured batches.

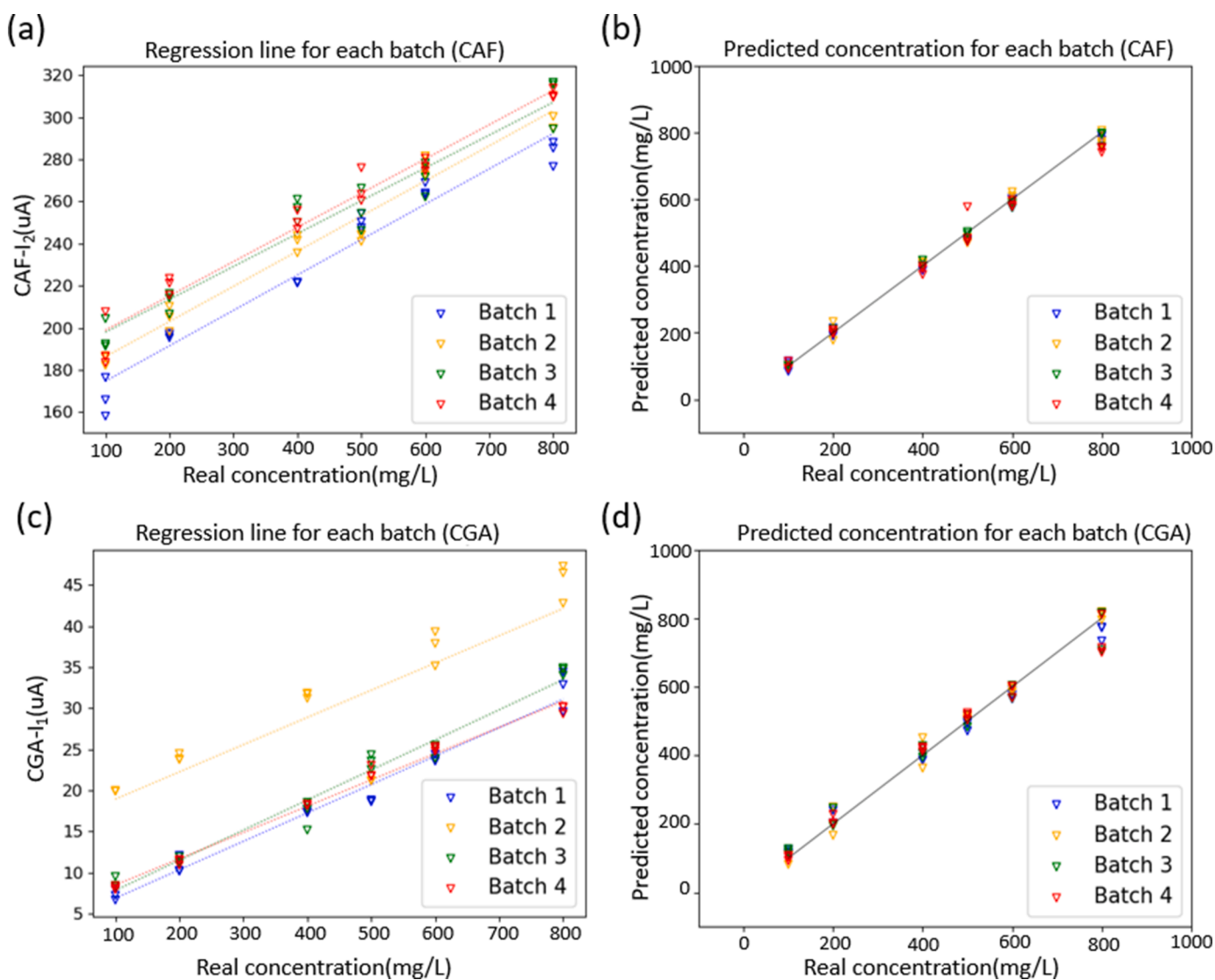


Fig. 7. (a) Linear regression lines for CAF measurements from different batches, (b) predicted results for CAF measurements from different batches using the ANN model, (c) linear regression lines for CGA measurements from different batches, (d) predicted results for CGA measurements from different batches using the ANN model.

To require the same sensing results in different batches of sensors, the design codes of different batches were entered into the device to calibrate the results after measurements. It is a well-known method for commercial electrochemical sensors. Unique chemical reactions were performed in this study. The CAF reaction can be enhanced using a 0.1 M sulfuric solution. Although the CAF signal can be enlarged with this method, a nonuniform electrochemical double layer was formed when sulfuric acid contacted the electrodes. The different contact times caused the varying thicknesses of the electrochemical double layers, which formed near the electrodes. The electrochemical plots were shifted by this interference.

3.3. ANN model developed for different waiting times

In this study, we also investigated the impact of different waiting times on the sensors. Varied waiting times could produce alterations in the interface morphology of the double layer on the surface of the sensor. Fig. 8(a) illustrates the plots obtained for samples with waiting times of 0, 30, 60, 180 and 300 s using LSV, whereas Fig. 8(b) presents the plots obtained using DPV. Notably, both LSV and DPV plots exhibit distinct electrochemical features for different waiting times. Additionally, considerable shifts in the peaks are observed in both types of plots for different waiting times. The time required for the solution to fully cover the electrochemical electrodes on the sensing area of the sensor should be considered. This is remarkable due to variations in waiting times among different individuals and the limitations of operating conditions. It is crucial to acknowledge the impact of waiting time as it can affect the accuracy of CAF and CGA measurements. In our study, we observed poor accuracy when different waiting times were considered. No potential difference was applied on the sample during the waiting time.

The ANN model was developed to reduce the sensing deviations of CGA and CAF in this study. We tested 500 mg/L CAF and CGA samples each to determine the uniformity of the sensing results. Before applying the ANN model, the deviation was large at each waiting time, and the different waiting times produced different sensing results in the same solution. After applying the ANN model, the deviation reduced at each waiting time, and the CAF and CGA predictions became more consistent. The comparison is shown in Fig. 9.

3.4. Discussion

The linear calibration line equation is a common method for predicting unknown sample concentrations. However, the predicted results of the coffee sample were poor. Table 3 show that the RMSE and MAE of the CAF test set were 59.38 and 47.80, respectively. Table 4 show that the RMSE and MAE of the CGA test set were 36.74 and 26.84, respectively. The accuracy of CAF was 15.3%, and that of CGA was 32.7%. Zaho [21] reported a method, which combines random forest and linear equations to analyze glucose and insulin in serum. This method was employed to predict CAF and CGA concentrations. After Zaho's model was built by the training set, we compared the test set results to determine the most suitable model for the coffee sample. Table 3 show that the RMSE and MAE of the CAF test set were 15.08 and 12.02, respectively. Table 4 show that the RMSE and MAE of the CGA test set were 24.63 and 16.28, respectively. The accuracy of CAF was 76.3%, and that of CGA was 53.9%, respectively. After applying the ANN models to analyze the coffee sample, the RMSE and MAE of CAF test were 10.20 and 7.00 Table 3, respectively. The RMSE and MAE of CGA test were 4.48 and 6.31 in Table 4, respectively. The accuracy of CAF reached 92.4%, and that of CGA reached 90.6% in this work. Tables 3 and 4 show the prediction results using different models.

4. Conclusion

The requirements for measuring CAF and CGA are rising and traditional methods, such as HPLC, are time-consuming and expensive. Electrochemical methods enable a short sensing time. CAF and CGA were both detected in 20 s in this study. Considering that the electrochemical measurement requires the extra potential to simulate specific chemical reactions, the minute different uniformities of electrochemical sensors can generate different results in the same sample. The different batches of sensors and different waiting times were two major challenges discussed in this paper. The ANN models were developed after machine learning. The ANN models prevented noise interference and predicted accurate results. After applying the ANN models to analyze the coffee sample, the accuracy of CAF reached 92.4%, and that of CGA reached 90.6%. The ANN models also solved the problem of unstable quality among different batches of sensors. The different thicknesses of the electrochemical double layer formed because the operator could not control the dropping method to be the same every time. The ANN models helped to reduce uncontrollable variables to achieve the same

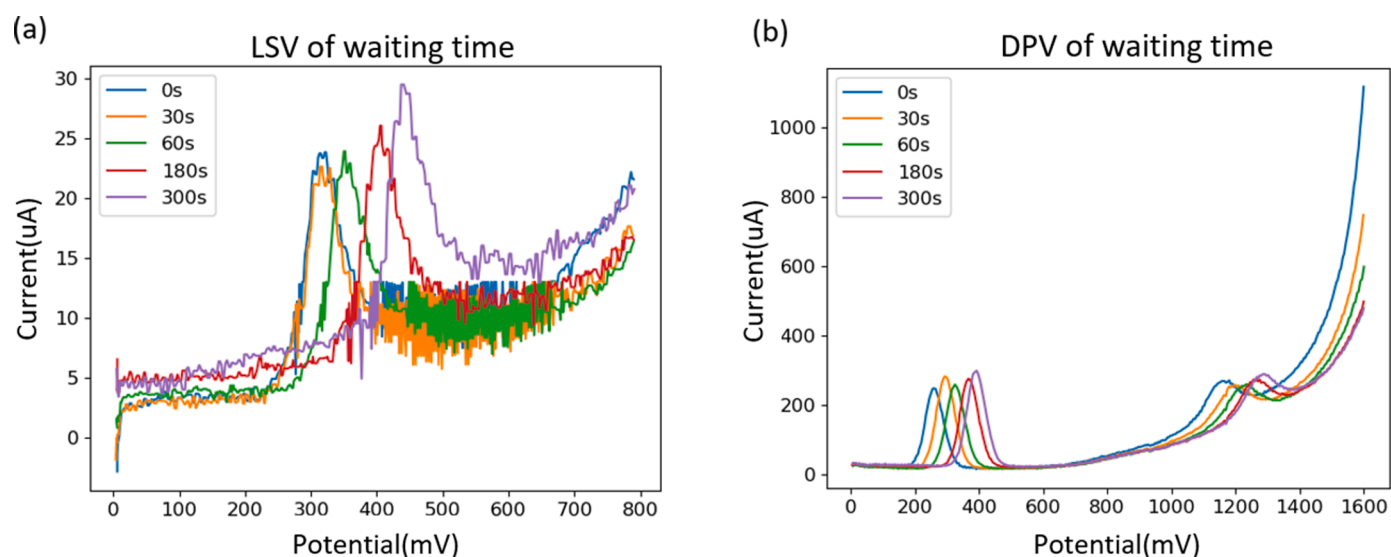


Fig. 8. (a) LSV measurement plots for samples with different waiting times of 0, 30, 60, 180, and 300 s. (b) DPV measurement plots for samples with different waiting times of 0, 30, 60, 180 and 300 s.

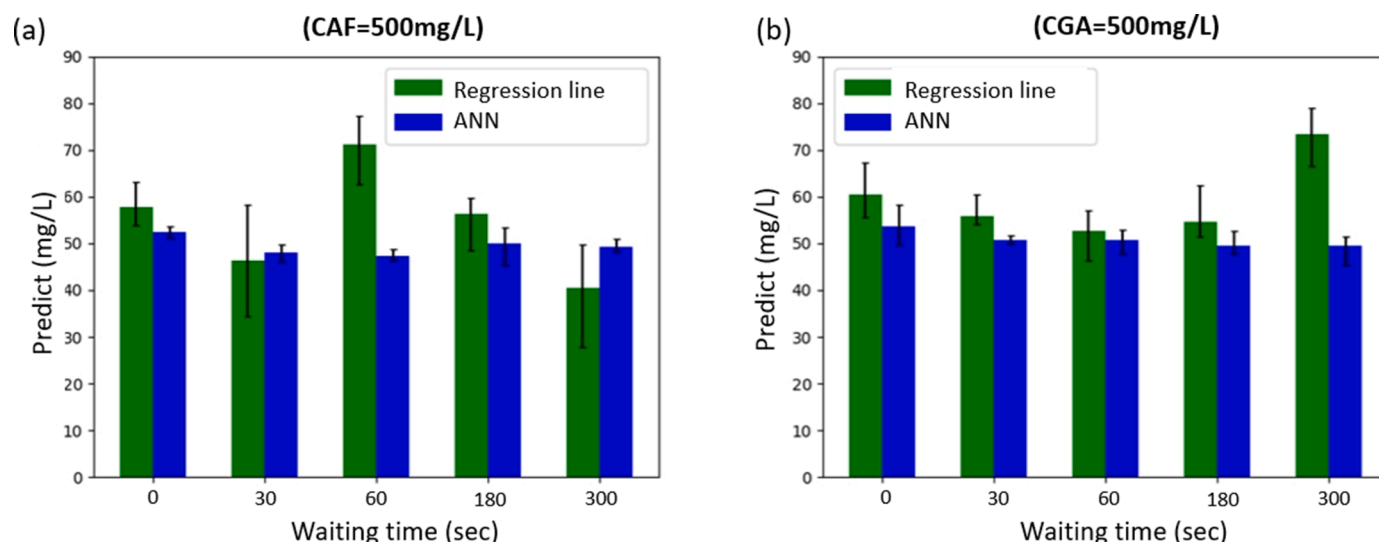


Fig. 9. Prediction results for (a)CAF measurements and (b) CGA measurements using the calibration line method and ANN model for waiting times of 0, 30, 60, 180, and 300 s.

Table 3

Comparison of different models for CAF measurement using the calibration line, RF, and ANN model.

Analysis model	MAE	RMSE	Accuracy (%)
Calibration line model	47.80	59.38	15.3
RF model [21]	12.02	15.08	76.3
ANN model (this study)	7.00	10.20	92.4

Table 4

Comparison of different models for CGA measurement using the calibration line, RF, and ANN model.

Analysis model	MAE	RMSE	Accuracy (%)
Calibration line model	26.84	36.74	32.7
RF model [21]	16.28	24.63	53.9
ANN model (this study)	6.31	4.48	90.6

sensing results. The method can be used to detect CAF and CGA with accuracy. It also enhances other electrochemical sensors by improving the measurement error for commercial products.

Ethical approval

This article does not contain any studies with human participants or animals performed by any of the authors.

Funding

This work was financially supported by the “Innovation and Development Center of Sustainable Agriculture” from The Featured Areas Research Center Program within the framework of the Higher Education Sprout Project by the Ministry of Education (MOE) in Taiwan. This research is also supported (in part) by National Science and Technology Council (NSTC) of Taiwan under grant numbers under grant numbers MOST 110-2221-E-005-073, MOST110-2622-E-018-004, MOST 111-2218-E-005-011, and NSTC 111-2634-F-005-001 project Smart Sustainable New Agriculture Research Center (SMARTer).

CRedit authorship contribution statement

Bing-Chen Gu: Conceptualization, Investigation, Data curation,

Writing – original draft. **Kuan-Jung Chung:** Conceptualization, Methodology, Project administration, Funding acquisition. **Bo-Wei Chen:** Investigation, Data curation, Writing – original draft. **Yu-Han Dai:** Investigation, Data curation. **Chia-Che Wu:** Conceptualization, Methodology, Validation, Formal analysis, Resources, Writing – original draft, Writing – review & editing, Project administration, Funding acquisition.

Declaration of Competing Interest

The authors declare that they have no known competing financial interests or personal relationships that could have appeared to influence the work reported in this paper.

Data availability

Data will be made available on request.

Acknowledgements

We thank the NSTC and MOE in Taiwan for funding this work.

Reference

- [1] K.L. Johnston, M.N. Clifford, L.M. Morgan, Coffee acutely modifies gastrointestinal hormone secretion and glucose tolerance in humans: glycemic effects of chlorogenic acid and caffeine, *Am. J. Clin. Nutr.* 78 (4) (2003) 728–733.
- [2] M. Rubach, et al., A dark brown roast coffee blend is less effective at stimulating gastric acid secretion in healthy volunteers compared to a medium roast market blend, *Mol. Nutr. Food Res.* 58 (6) (Jun 2014) 1370–1373.
- [3] E. Ergin, O. Tokusoglu, H. Vural, Coffee toxicology, processing of the coffee and liver diseases (is it a miracle of nature?), *J. Food Process Preserv.* 45 (4) (2021).
- [4] J. Zuo, W. Tang, Y. Xu, Anti-hepatitis B virus activity of chlorogenic acid and its related compounds. *Coffee in Health and Disease Prevention*, Elsevier, 2015, pp. 607–613.
- [5] A. Shishov, N. Volodina, D. Nechaeva, S. Gagarinova, A. Bulatov, An automated homogeneous liquid-liquid microextraction based on deep eutectic solvent for the HPLC-UV determination of caffeine in beverages, *Microchem. J.* 144 (2019) 469–473.
- [6] R.D.C. Lopez-Sanchez, V.J. Lara-Diaz, A. Aranda-Gutierrez, J.A. Martinez-Cardona, J.A. Hernandez, HPLC method for quantification of caffeine and its three major metabolites in human plasma using fetal bovine serum matrix to evaluate prenatal drug exposure, *J. Anal. Methods Chem.* 2018 (2018), 2085059.
- [7] D.L.O. Ramos, M.M.A.C. Ribeiro, R.A.A. Munoz, E.M. Richter, Portable amperometric method for selective determination of caffeine in samples with the presence of interfering electroactive chemical species, *J. Electroanalytic. Chem.* 906 (2022).

- [8] W. Xu, et al., Make caffeine visible: a fluorescent caffeine "traffic light" detector, *Sci. Rep.* 3 (2013) 2255.
- [9] E. Bernalte, C. Marin Sanchez, E. Pinilla Gil, Determination of mercury in ambient water samples by anodic stripping voltammetry on screen-printed gold electrodes, *Anal. Chim. Acta* 689 (1) (2011) 60–64. Mar 9.
- [10] O. Dominguez Renedo, M.J. Arcos Martinez, Anodic stripping voltammetry of antimony using gold nanoparticle-modified carbon screen-printed electrodes, *Anal. Chim. Acta* 589 (2) (2007) 255–260. Apr 25.
- [11] Y. Tadesse, A. Tadese, R.C. Saini, R. Pal, Cyclic voltammetric investigation of caffeine at anthraquinone modified carbon paste electrode, *Int. J. Electrochem.* 2013 (2013) 1–7.
- [12] J.Y. Sun, K.J. Huang, S.Y. Wei, Z.W. Wu, F.P. Ren, A graphene-based electrochemical sensor for sensitive determination of caffeine, *Colloids Surf. B Biointerfaces* 84 (2) (2011) 421–426. Jun 1.
- [13] Y.-J. Fan, Y.-C. Hsu, B.-C. Gu, C.-C. Wu, Voltammetric measurement of *Escherichia coli* concentration through p-APG hydrolysis by endogenous β -galactosidase, *Microchem. J.* 154 (2020).
- [14] B.Y. Wang, B.C. Gu, G.J. Wang, Y.H. Yang, C.C. Wu, Detection of Amyloid-beta(1-42) aggregation with a nanostructured electrochemical sandwich immunoassay biosensor, *Front. Bioeng. Biotechnol.* 10 (2022), 853947.
- [15] J. Kozak, K. Tyszczyk-Rotko, M. Wojciak, I. Sowa, M. Rotko, First screen-printed sensor (Electrochemically activated screen-printed boron-doped diamond electrode) for quantitative determination of rifampicin by adsorptive stripping voltammetry, *Materials (Basel)* 14 (15) (Jul 29 2021).
- [16] L. Chen, K. Chaisiwamongkhol, Y. Chen, R.G. Compton, Rapid electrochemical detection of vanillin in natural vanilla, *Electroanalysis* 31 (6) (2019) 1067–1074.
- [17] Z.J. Han, R. Morrow, B.K. Tay, D. McKenzie, Time-dependent electrical double layer with blocking electrode, *Appl. Phys. Lett.* 94 (4) (2009).
- [18] M.I. Jordan, T.M. Mitchell, Machine learning: trends, perspectives, and prospects, *Science* 349 (6245) (2015) 255–260.
- [19] P. Puthongkham, S. Wirojsaengthong, A. Suea-Ngam, Machine learning and chemometrics for electrochemical sensors: moving forward to the future of analytical chemistry, *Analyst* 146 (21) (2021) 6351–6364. Oct 25.
- [20] A. Mistry, A.A. Franco, S.J. Cooper, S.A. Roberts, V. Viswanathan, How machine learning will revolutionize electrochemical sciences, *ACS Energy Lett.* 6 (4) (Apr 9 2021) 1422–1431.
- [21] Y. Zhao, et al., AI powered electrochemical multi-component detection of insulin and glucose in serum, *Biosens. Bioelectron.* 186 (May 1 2021), 113291.
- [22] D.E. Blanco, B. Lee, M.A. Modestino, Optimizing organic electrosynthesis through controlled voltage dosing and artificial intelligence, *Proc. Natl. Acad. Sci. U. S. A.* 116 (36) (Sep 3 2019) 17683–17689.
- [23] O. Alharbi, Y. Xu, R. Goodacre, Simultaneous multiplexed quantification of caffeine and its major metabolites theobromine and paraxanthine using surface-enhanced Raman scattering, *Anal. Bioanal. Chem.* 407 (27) (Nov 2015) 8253–8261.
- [24] H. Chen, D. Li, E. Katelhon, R. Miao, R.G. Compton, Experimental voltammetry analyzed using artificial intelligence: thermodynamics and kinetics of the dissociation of acetic acid in aqueous solution, *Anal. Chem.* 94 (15) (Apr 19 2022) 5901–5908.
- [25] K.Y. Tajeu, E. Ymele, S.L. Zamboujiokeng, I.K. Tonle, Electrochemical sensor for caffeine based on a glassy carbon electrode modified with an Attapulgite/nafion film, *Electroanalysis* (2018).
- [26] M. Namazian, H.R. Zare, Electrochemistry of chlorogenic acid: experimental and theoretical studies, *Electrochim. Acta* 50 (22) (2005) 4350–4355.
- [27] K. Hara, D. Saito, H. Shouno, Analysis of function of rectified linear unit used in deep learning, in: 2015 International Joint Conference on Neural Networks (IJCNN), IEEE, 2015, pp. 1–8.
- [28] S. Balasundaram, S.C. Prasad, Robust twin support vector regression based on Huber loss function, *Neural Comput. Appl.* 32 (15) (2019) 11285–11309.
- [29] E.M. Dogo, O.J. Afolabi, B. Twala, On the relative impact of optimizers on convolutional neural networks with varying depth and width for image classification, *Appl. Sci.* 12 (23) (2022).
- [30] by I. Halperin, Reinforcement learning and stochastic optimization: a unified framework for sequential decisions, in: Warren B. Powell (Ed.), Wiley, 2022.